Organic Electronics 56 (2018) 170–177

Contents lists available at ScienceDirect

Organic Electronics

journal homepage: www.elsevier.com/locate/orgel

Multifunctional sensor based on organic field-effect transistor and ferroelectric poly(vinylidene fluoride trifluoroethylene)

Stuart Hannah[a], Alan Davidson[a], Ivan Glesk[a], Deepak Uttamchandani[a], Ravinder Dahiya[b], Helena Gleskova[a,*]

[a] Department of Electronic and Electrical Engineering, University of Strathclyde, Glasgow, G1 1XW, United Kingdom
[b] School of Engineering, University of Glasgow, James Watt South Building, Glasgow G12 8QQ, United Kingdom

ARTICLE INFO

Keywords:
Sensor
Capacitance
P(VDF-TrFE)
Organic transistor
Force
Temperature

ABSTRACT

A multifunctional sensor that responds to all – static/quasi-static or dynamic temperature or force – is reported. The sensor is based on a ferroelectric poly(vinylidene fluoride trifluoroethylene) (P(VDF-TrFE)) capacitor connected to the gate of organic field-effect transistor (OFET). Both, the P(VDF-TrFE) capacitance and the output voltage of the P(VDF-TrFE)/OFET sensor exhibit a logarithmic response to static compressive force, leading to higher sensitivity for small forces. In addition, both the P(VDF-TrFE) capacitance and the output voltage of the P(VDF-TrFE)/OFET sensor exhibit a linear dependence on the static/constant temperature. Response to static force or temperature is observed irrespective of whether P(VDF-TrFE) is in ferroelectric or paraelectric states, confirming that piezo/pyroelectricity is not essential when monitoring static events. The piezo/pyroelectricity become activated during dynamic events (dynamic force or temperature) when the ferroelectric P(VDF-TrFE)/OFET sensor is used. The obtained results indicate different sensing mechanisms for static and dynamic stimuli. Consequently, by choosing P(VDF-TrFE) layers in ferroelectric or paraelectric states a route for differentiating between the static and dynamic stimuli may exist.

1. Introduction

The field of tactile sensing has been growing rapidly in recent years and applications span from touch screen interfaces to electronic skin (e-skin) for humanoid robots and electronic textiles (e-textiles). An e-skin is expected to replicate the complex sensory response of real skin, e.g. pressure and temperature transduction, and also possess the ability to stretch and conform to non-planar surfaces [1]. Consequently the demand for multimodal sensing (sensing of various stimuli) and surface mapping (number of sensors per unit area) favors sensor arrays, i.e. arrays of pixels that contain sensing devices for targeted external stimuli. On the other hand, discrete unobtrusive sensors placed in garments at specific body locations are suitable for electronic textile applications. Examples include physiological sensors (sensing body's physiological state), bio-kinetic sensors (tracking individual's movement), and ambient sensors (impact of the environment on the individual).

Thin-film sensors for pressure/force/strain or temperature have been the focus of many recent research activities aimed at e-skin or e-textiles. For pressure/force/strain detection they exploit the piezo-resistive effect [2–4], the piezoelectric effect [5–8] or capacitive changes [9,10], whereas for temperature sensing capacitive [11] and pyroelectric-based sensors [12] can be found.

To harvest the response of certain materials to pressure/force/strain or temperature stimuli, the sensors often contain field-effect transistors (FETs) that convert the response generated by the material to an amplified voltage signal, suitable for subsequent interfacing with readout electronics [4,7,8,13–19]. Here, ferroelectric polymers are very attractive because they exhibit piezo- and pyro-electric properties, while being inherently compatible with plastic substrates. Some examples of previous work include a polyvinylidene difluoride (PVDF) capacitor combined with an organic charge-modulated FET for the detection of dynamic force [13] or changing temperature [14], a poly(vinylidene fluoride trifluoroethylene) (P(VDF-TrFE)) capacitor combined with an organic electrochemical transistor for contactless touch detection [15], or P(VDF-TrFE) layer integrated with a CMOS FET to form a piezoelectric oxide semiconductor field-effect transistor (POSFET) for touch sensing [17]. In these devices, the piezoelectric or pyroelectric properties of the ferroelectric polymers have been exploited, allowing sensing of the dynamic/changing force or temperature. A human skin, however, is able to detect static/constant as well as dynamic/changing stimuli, and distinguish between them. Temperature measurements

* Corresponding author. Department of Electronic and Electrical Engineering, University of Strathclyde, Royal College, 204 George Street, Glasgow, G1 1XW, United Kingdom.
E-mail address: helena.gleskova@strath.ac.uk (H. Gleskova).

https://doi.org/10.1016/j.orgel.2018.01.041
Received 23 May 2017; Received in revised form 29 December 2017; Accepted 30 January 2018
Available online 11 February 2018

may also involve detection of static/constant stimuli since temperature changes may be occurring on long time scales. Therefore, it would be desirable if the sensors utilizing P(VDF-TrFE) would provide the measurement of both the static and dynamic stimuli.

Previously, we have reported that the capacitance of a ferroelectric P(VDF-TrFE) layer changes with force or temperature [20]. In addition, the ferroelectric co-polymer exhibits piezo- and pyroelectric properties. In this paper we present a sensor based on a P(VDF-TrFE) capacitor and a low-voltage organic field-effect transistor that responds to static/quasi-static force or temperature. Having the ability to also respond to dynamic force or temperature, such sensor offers the desired multi-functionality. The use of one single material, such as P(VDF-TrFE), also lends a major advantage during the fabrication.

2. Experimental procedures

Parallel-plate capacitors containing a 2.5-μm-thick P(VDF-TrFE) (Piezotech) layer sandwiched between two metal layers (Al and Au) were fabricated using the procedure described previously [21]. The crystalline structure, and consequently the piezoelectric and pyroelectric properties of the polymer film, depend on the molecular proportion x ($0.6 < x < 0.85$) of vinyledene fluoride in P(VDF_x-$TrFE_{1-x}$). Among various compositions of P(VDF-TrFE), the one with 65/35 wt ratio exhibits good ferroelectric response [22]. For this reason, P(VDF-TrFE) with 65/35 wt ratio was used in this work. A 10% P(VDF-TrFE) solution was spin coated at 3000 rpm for 30 s. Afterwards the polymer films were annealed to enhance the crystallization, to evaporate any left-over solvent and to remove any local stress generated during deposition. The films were annealed close to the melting point of P(VDF-TrFE), i.e. the temperature was ramped to 155 °C for 1 h, kept at 155 °C for 10 min, and then gradually lowered to room temperature in 4 h to minimise the stress. After the annealing, the polymer films were treated with hexamethyldisilazane (HMDS) followed by vacuum deposition of a 200-nm-thick top metal layer composed of thin Cr and thick Au. After fabrication, the capacitor was subjected to DC poling to induce the ferroelectric phase and subsequently mounted onto a glass slide for compatibility with the force testing equipment. Poling of P(VDF-TrFE) was achieved by applying a high electric field (100 V/μm) across its thickness in multiple steps as explained in Ref. [21]. The relative permittivity of such P(VDF-TrFE) was about 10.

Bottom-gate, top-contact p-channel OFETs based on dinaphtho[2,3-b:2′,3′-*f*]thieno[3,2-*b*]thiophene (DNTT) (Sigma Aldrich) were fabricated according to the procedure described in Ref. [23]. The bi-layer gate dielectric consists of aluminum oxide (AlO_x) prepared by UV/ozone oxidation and an alkyl phosphonic acid (C_nPA) (Strem Chemicals) monolayer prepared in vacuum. Transistors with $C_{14}PA$, $C_{16}PA$, and $C_{18}PA$ have been used, thereby allowing us to test the sensor functionality for a range of field-effect mobilities and threshold voltages [23]. The mobility of the transistors used in this study varied between 0.02 and 0.56 cm^2/Vs and the threshold voltage between −0.19 and −0.68 V. Fig. 1(a) shows the Al/AlO_x/C_nPA/DNTT/Au transistor structure. The transistors had nominal channel length of 30 μm and a channel width of 1 mm.

To finalize the sensor, P(VDF-TrFE) capacitor was connected to OFET gate electrode by gold wire. Unless otherwise noted, the Al electrode of P(VDF-TrFE) was connected to the gate. Fig. 1(b) shows the cross-section of the P(VDF-TrFE) capacitor with an area of 5 by 5 mm^2 and Fig. 1(c) presents the circuit diagram of the P(VDF-TrFE)/OFET sensor. To take advantage of the low-voltage transistor, the voltages were kept as low as possible. The drain (V_D) was always biased at −2 V. V_{IN} was chosen just high enough to allow the transistor to operate in saturation. The output voltage V_{OUT} was measured across the 1 MΩ resistor. In some instances, the voltage on the gate of the transistor V_G was also measured. The sensor measurements were performed in ambient atmosphere and therefore, the OFET transfer characteristics were also recorded under ambient light.

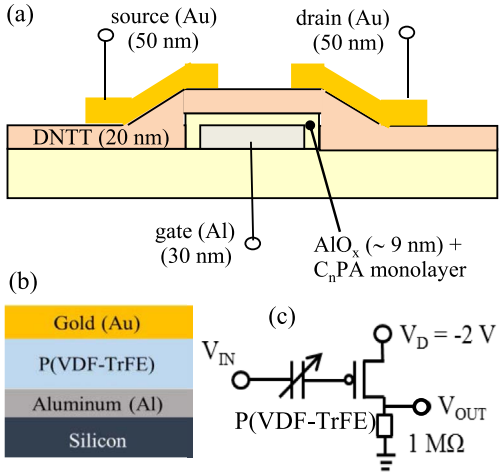

Fig. 1. Cross-sectional view of OFET (a) and P(VDF-TrFE) capacitor (b); schematic of the P(VDF-TrFE)/OFET sensor (c).

Static compressive force of up to ~9 N was applied in the normal direction to the P(VDF-TrFE) capacitor. Force was applied using a linear stage controlled by a stepper motor (Zaber Technologies) fitted with an in-house designed Teflon probe capable of compressing 40% of the capacitor's active area. Force was recorded with a load cell (Omega) and extracted after it had stabilized. All experiments were performed at room temperature. The minimum and maximum applied force was ~80 mN and ~9 N, respectively. Capacitance of a stand-alone P(VDF-TrFE) capacitor and V_{OUT} of a P(VDF-TrFE)/OFET sensor were measured as functions of the applied force. The output voltage V_{OUT} was referenced to the value of $V_{OUT} = V_{REF}$ with no force applied. $|\Delta V_{OUT}| = |V_{OUT} - V_{REF}|$ was calculated and plotted as a function of force. Measurements were also performed on a P(VDF-TrFE)/OFET sensor where the P(VDF-TrFE) capacitor was depoled by heating at 125 °C for 30 min (T_{Curie} ~ 110 °C) to induce a paraelectric state. The disappearance of the ferroelectric phase, i.e. piezoelectric and pyroelectric properties, was verified with a charge amplifier.

Similarly to the static force experiments, the stand-alone P(VDF-TrFE) capacitor and P(VDF-TrFE)/OFET sensor were studied as a function of P(VDF-TrFE) temperature. The temperature was applied to P(VDF-TrFE) capacitor via a Peltier element that was connected to a custom designed PID controller and LabView program. Temperatures in the range from ~20 to ~50 °C were used. No force was applied to P(VDF-TrFE) during the temperature experiments.

The electrical measurements were performed with Agilent B1500A semiconductor parameter analyzer equipped with a capacitance module. Capacitance was measured as a function of frequency and extracted at 2 kHz.

3. Results

3.1. Response of P(VDF-TrFE)/OFET sensor to static force

Fig. 2(a) shows the change in P(VDF-TrFE) capacitance when compressive static force is applied in the normal direction to a poled P(VDF-TrFE) capacitor. The capacitance is 858.6 pF when no force is applied. It rises with the increasing applied force and reaches a value of 886.9 pF at 8.85 N. The capacitance increases logarithmically, resulting in a larger change for low forces. If one defines the sensitivity as a change in capacitance per unit force, a sensitivity of ~7.5 pF/N is observed in the range from 0 to ~0.5 N. Fig. 2(b) shows the response of P(VDF-TrFE)/OFET sensor when a static force of 0.74 N lasting ~ 7 s is repeatedly applied to P(VDF-TrFE). Both the transistor drain current I_D and V_{OUT} are shown. Application of 0.74 N leads to a change in V_{OUT} of

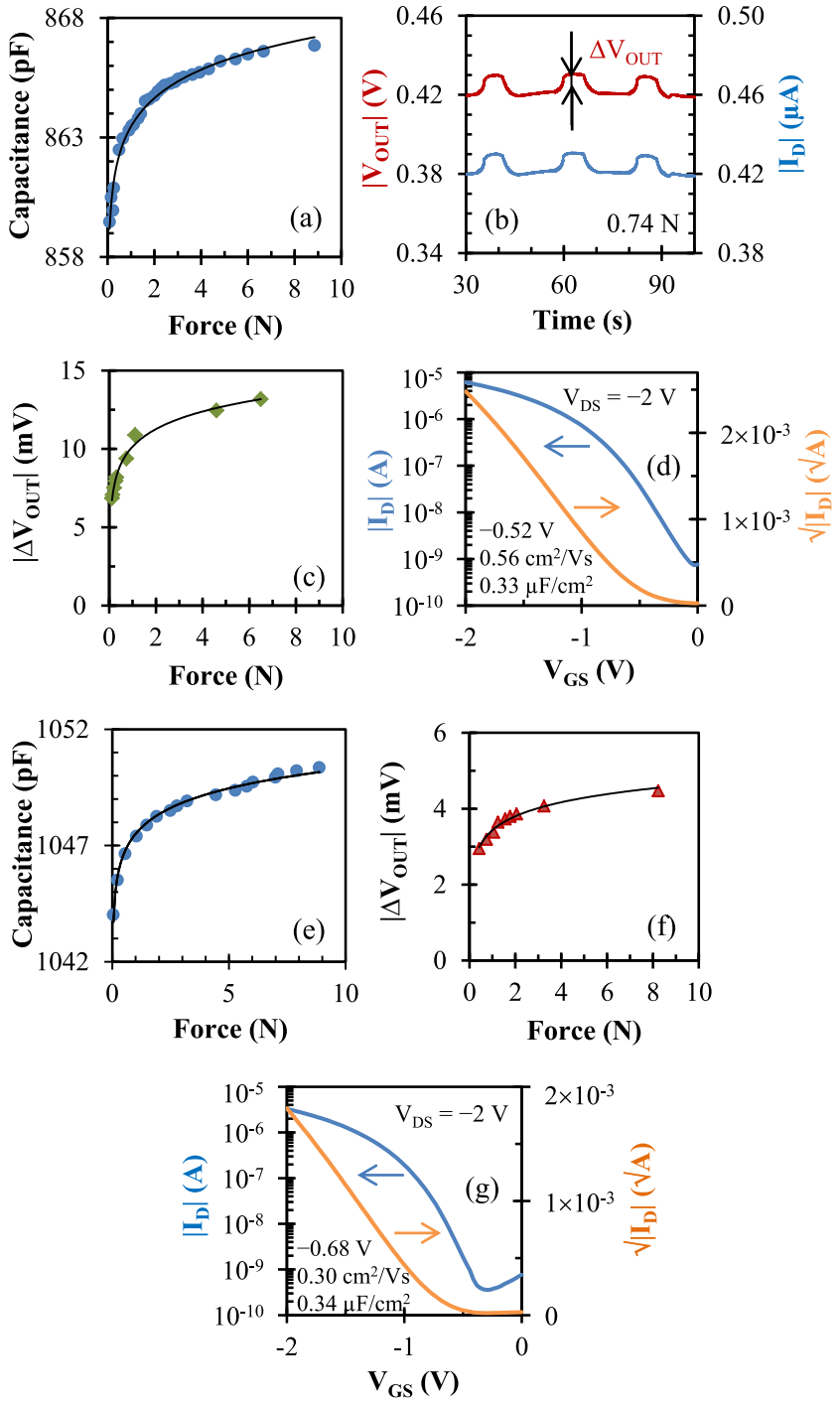

Fig. 2. Effect of force on *poled* (a)–(d) and *depoled* (e)–(g) P(VDF-TrFE). P(VDF-TrFE) capacitance as a function of applied force (a, e); force of 0.74 N applied repeatedly to P(VDF-TrFE)/OFET sensor (b); $|\Delta V_{OUT}|$ as a function of force applied to P(VDF-TrFE)/OFET sensor (c, f); corresponding OFET transfer characteristic in saturation regime (d, g). OFET threshold voltage, field-effect mobility and gate dielectric capacitance are given in (d) and (g).

9.4 mV. Fig. 2(c) shows the change in $|V_{OUT}|$ of the P(VDF-TrFE)/OFET sensor for forces ranging from 0 to 6.5 N. $|\Delta V_{OUT}|$ increases logarithmically as a function of applied force. For forces less than 0.1 N a high sensitivity of ~65 mV/N is observed. In the range from 0.1 N and 1 N, the sensitivity is reduced to ~3.9 mV/N. Finally, Fig. 2(d) shows the transfer characteristic in the saturation regime of the transistor used in the sensor.

To investigate the mechanism behind the change in V_{OUT}, the P(VDF-TrFE) capacitor was depoled to bring it to a paraelectric state and thus eliminate its piezoelectric properties. Fig. 2(e) shows the change in P(VDF-TrFE) capacitance when compressive static force is applied in the normal direction to the depoled P(VDF-TrFE) capacitor. The capacitance is 1043.2 pF when no force is applied. It rises with the increasing applied force and reaches a value of 1050.4 pF at 8.87 N. The capacitance increases logarithmically and the effect of the force is similar to that of the poled P(VDF-TrFE). Fig. 2(f) shows the change in V_{OUT} of the depoled P(VDF-TrFE)/OFET sensor for forces ranging from 0 to 8 N. Again, $|\Delta V_{OUT}|$ increases logarithmically as a function of applied force. Fig. 2(f) confirms that the change in the output voltage does not arise from the piezoelectric effect. For both the poled and depoled P

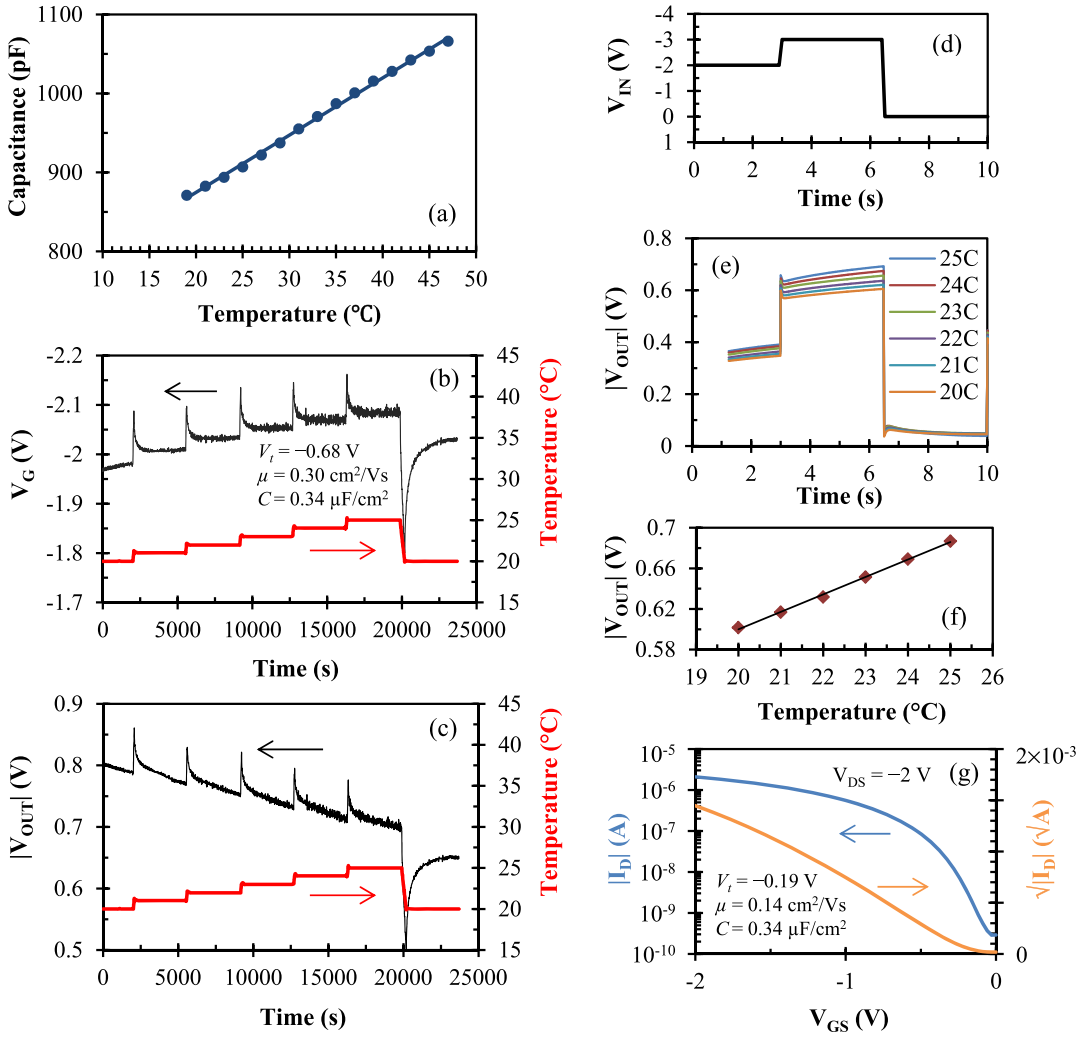

Fig. 3. Effect of temperature on *poled* P(VDF-TrFE)/OFET sensor with constant (b,c) and pulsed (d–f) input voltage. P(VDF-TrFE) capacitance as a function of temperature (a); V_G (b) and $|V_{OUT}|$ (c) as functions of time; pulsed V_{IN} (d); $|V_{OUT}|$ for temperatures between 20 and 25 °C (e); and $|V_{OUT}|$ as a function of temperature extracted from part e (f). OFET transfer characteristic for sensor with constant or pulsed input V_{IN} is shown in Fig. 2(g) and 3(g), respectively.

(VDF-TrFE), the logarithmic sensor response means that the sensitivity decreases as the force increases, providing much higher sensitivity for forces below 0.1 N. Finally, if one compares $|\Delta V_{OUT}|$ between Fig. 2(c) and (f), it can be seen that it is smaller for the latter. This is attributed to an OFET having lower field-effect mobility and higher threshold voltage than the OFET used in Fig. 2(c). Fig. 2(g) shows the transfer characteristic in the saturation regime of the transistor used in the depoled P(VDF-TrFE)/OFET sensor.

3.2. Response of P(VDF-TrFE)/OFET sensor to static/constant temperature

Fig. 3(a) shows the change in capacitance of the poled P(VDF-TrFE) capacitor for temperatures between 19 and 47 °C. The capacitance increases linearly with temperature as a result of rising relative permittivity. Defining sensitivity as a change in capacitance per degree Celsius, the capacitor displays sensitivity of 7.25 pF/°C. Fig. 3(b) and (c) show the response of a poled P(VDF-TrFE)/OFET sensor to constant temperature. The P(VDF-TrFE) temperature was increased from 20 to 25 °C in 1 °C increments, and each temperature was held constant for ~ 1 h. After waiting for 1 h at the final temperature (25 °C), the temperature was returned to 20 °C in a single step. The sensor was biased for 10,000 s at 20 °C before the temperature ramp was applied. Fig. 3(b) and (c) show V_G and $|V_{OUT}|$ as functions of time along with the associated temperature profile. V_G increases with increasing temperature and remains constant when the temperature is held constant. When the temperature set point is changed, the temperature requires approximately 5 min to stabilize. V_G takes longer to stabilize; however, once stabilized, it remains constant until the next change in the temperature occurs. The characteristic of the OFET in saturation is shown in Fig. 2(g).

Over the 5 °C temperature range, V_G shows linear response to temperature with a sensitivity of ~20.5 mV/°C. However, over extended period of time, OFET drain current I_D gradually decreases as a result of the transistor bias stress effect, resulting in a reduction in $|V_{OUT}|$. This can be inferred from the black curve shown in Fig. 3(c).

By definition, "static" temperature does not undergo sudden changes and therefore infrequent sampling using voltage pulses on the input would provide a temperature reading whilst significantly reducing the effect of bias stress in the OFET. To investigate this, an AC pulse from 0 to −3 V with a period of 10 s was used for V_{IN}. The pulse included a pre-bias step at −2 V before being ramped to −3 V (see Fig. 3(d)). Fig. 3(e) shows $|V_{OUT}|$ of the poled P(VDF-TrFE)/OFET sensor for temperatures between 20 and 25 °C. Fig. 3(f) presents $|V_{OUT}|$ extracted at V_{IN} = −3 V for various temperatures. $|V_{OUT}|$ increases linearly as a function of temperature between 20 and 25 °C and displays a sensitivity of 17.2 mV/°C. Finally, Fig. 3(g) shows the transfer characteristic of the OFET alone.

To confirm that the changes in $|V_{OUT}|$ shown in Fig. 3 were not

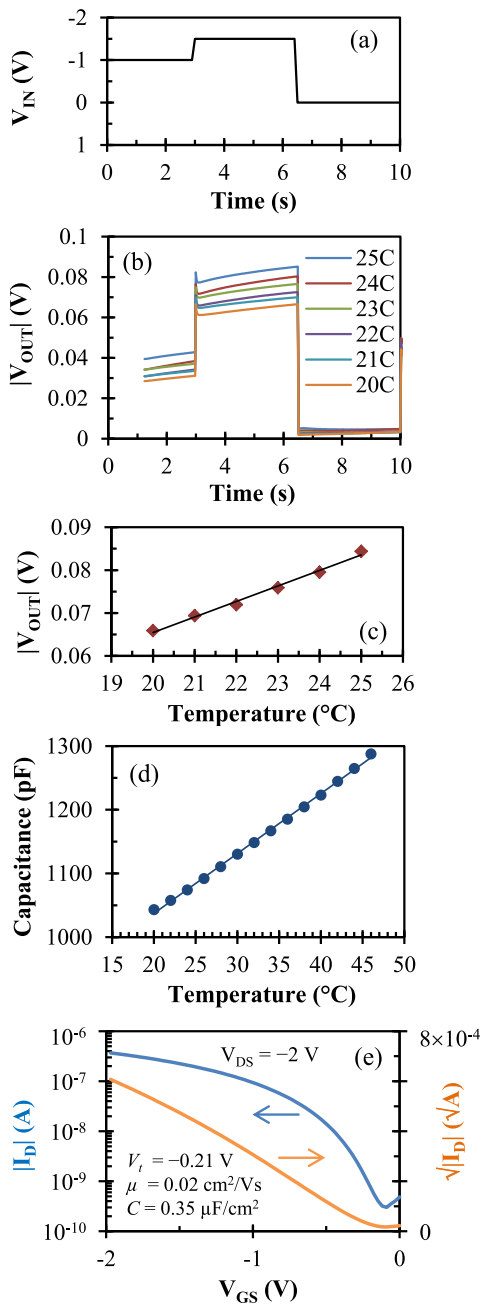

Fig. 4. Effect of temperature on *depoled* P(VDF-TrFE)/OFET sensor using pulsed input voltage. Pulsed V_{IN} (a); $|V_{OUT}|$ for temperatures between 20 and 25 °C (b); $|V_{OUT}|$ as a function of temperature extracted from part b (c); P(VDF-TrFE) capacitance as a function of temperature (d); and corresponding OFET transfer characteristic in saturation regime (e).

driven by the pyroelectricity of P(VDF-TrFE), a similar experiment was performed on a depoled P(VDF-TrFE)/OFET sensor. An AC pulse from 0 to −1.5 V with a period of 10 s was used for V_{IN}. The pulse included a −1 V pre-bias for 3 s before ramping to −1.5 V (see Fig. 4(a)). Fig. 4(b) shows $|V_{OUT}|$ of the depoled P(VDF-TrFE)/OFET sensor for a set of constant temperatures, using the pulsed input voltage. The temperature was varied from 20 to 25 °C, in 1 °C increments. $|V_{OUT}|$ was extracted at V_{IN} = −1.5 V for each temperature and the results are shown in Fig. 4(c). Fig. 4(d) shows the change in capacitance of the depoled P(VDF-TrFE) capacitor with temperature and Fig. 4(e) depicts the transfer characteristic of the OFET alone.

$|V_{OUT}|$ displays a linear dependence in the measured temperature range. This is in agreement with the results shown in Fig. 3 for the poled P(VDF-TrFE)/OFET sensor. The sensor output voltage displays a sensitivity of ~3.8 mV/°C. Referring to Figs. 3 and 4, $|V_{OUT}|$ is smaller for the latter depoled condition. However, for the depoled P(VDF-TrFE)/OFET sensor, OFET field-effect mobility was only ~ 15% of the value of the OFET used in Fig. 4. In addition, a smaller V_{IN} pulse was used and the transistor operated in the linear regime.

3.3. Response of P(VDF-TrFE)/OFET sensor to dynamic temperature

Next, the response of the P(VDF-TrFE)/OFET sensor to dynamic/changing temperature is presented. Two P(VDF-TrFE)/OFET sensors were studied. In the first case, the P(VDF-TrFE) capacitor was in the poled state, therefore in a ferroelectric state and possessing pyroelectric properties. In the second case the P(VDF-TrFE) capacitor has been depoled, hence in the paraelectric state and not possessing pyroelectric properties. The sensor temperature was repeatedly ramped up and down to allow the appearance of the pyroelectric effect, if any, and V_{OUT} was monitored.

Fig. 5(a) and (c) present how $|V_{OUT}|$ of both the poled and depoled P(VDF-TrFE)/OFET sensor responds to a temperature ramp from 20 to 30 °C, respectively. The temperature was ramped quickly up and down without stabilizing. $|V_{OUT}|$ was recorded in real time together with the associated temperature profile. Fig. 5(b) depicts the transfer characteristic of the OFET used in Fig. 5(a) while Fig. 5(d) depicts the transfer characteristic of the OFET used in Fig. 5(c).

The response of the depoled P(VDF-TrFE)/OFET sensor (see Fig. 5(c)) to temperature is much weaker than for the poled case (Fig. 5(a)), where the pyroelectric effect strongly controls the output voltage V_{OUT}. For the poled P(VDF-TrFE), $|V_{OUT}|$ changes by ~ 1.2 V, compared with ~60 mV variation for the depoled P(VDF-TrFE). Nevertheless, this 60 mV increase equates to sensitivity of 6 mV/°C in the measured temperature range from 20 to 30 °C.

4. Discussion

P(VDF-TrFE) capacitance displays logarithmic dependence on the applied compressive force up to 9 N. Consequently, the sensitivity is significantly enhanced for low forces (< 0.5 N), showing values of ~7.5 pF/N. High sensitivity for small forces is critical for robotic skin because the majority of manipulative everyday tasks performed by a humanoid robot requires forces less than 1 N [24,25]. The applied compressive force would lead to a reduction in the capacitor thickness and an increased capacitance. Considering the data of Fig. 2(a,e) and assuming an elastic response of P(VDF-TrFE) to compression, the observed change in the capacitance with force means that our P(VDF-TrFE) layer should exhibit Young's modulus of ~70 MPa. While Young's modulus of PVDF-based polymers depends on the blend and the composition of the polymer [26], modulus of ~650 MPa has been reported for pure PVDF. This value is much higher than the one estimated for our P(VDF-TrFE) layer based on capacitance measurements. Consequently, other factors seem responsible for the capacitance change, e.g. a less-than-1% increase in relative permittivity of P(VDF-TrFE) would account for the capacitance change of ~8 pF upon the application of compressive force of ~9 N.

The capacitance of the P(VDF-TrFE) also changes with temperature as a result of rising relative permittivity with increasing temperature. Sensitivity of the P(VDF-TrFE) capacitor in the temperature range from 19 to 47 °C is ~7 pF/°C. Changes in capacitance with force and temperature are significant enough to be exploited for the measurement of static/quasi-static force or temperature, thus widening the exploitation of P(VDF-TrFE) ferroelectrics beyond their piezoelectric and pyroelectric properties.

To provide a useful output voltage signal for further signal processing, the P(VDF-TrFE) capacitor was connected to the gate of an organic thin-film transistor. Response of both poled and depoled P(VDF-TrFE)/

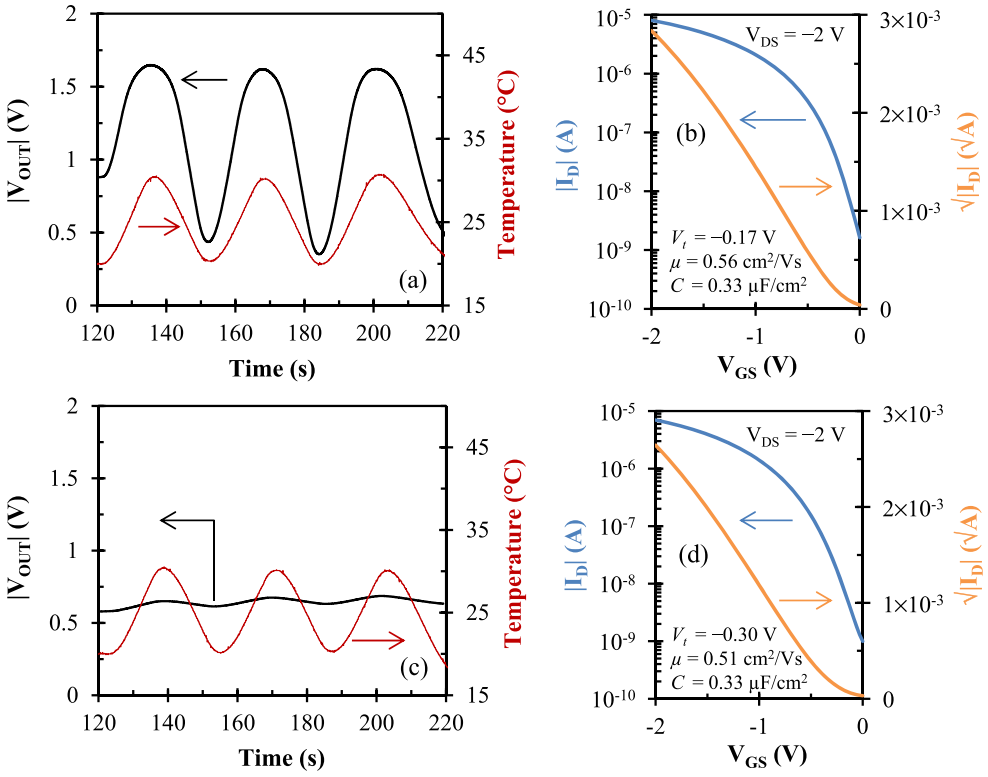

Fig. 5. Response of $|V_{OUT}|$ of P(VDF-TrFE)/OFET sensor to temperature variations between 20 and 30 °C for *poled* (a) and *depoled* (c) P(VDF-TrFE). The Au-side of P(VDF-TrFE) was connected to the gate of the transistor in (a). Corresponding OFET transfer characteristic in saturation regime for the *poled* (b) and *depoled* (d) P(VDF-TrFE)/OFET sensor.

OFET sensors were measured in a form of output voltage V_{OUT}. $|V_{OUT}|$ of both sensors responds logarithmically to normal compressive force (0–~8 N) applied to P(VDF-TrFE). This logarithmic dependence of $|V_{OUT}|$ is preserved regardless of the transistor parameters, i.e. the threshold voltage V_t and mobility μ. In Fig. 2, the P(VDF-TrFE)/OFET sensor that incorporates transistor with $\mu = 0.56$ cm^2/Vs and $V_t = -0.52$ V exhibits about a factor of three higher sensitivity when compared to the sensor using a transistor with $\mu = 0.30$ cm^2/Vs and $V_t = -0.68$ V. Assuming that the ferroelectricity does not affect $|V_{OUT}|$ during the measurement of static force, the transistor with higher μ and lower $|V_t|$ leads to higher sensitivity of the sensor and thus is more desirable.

Both the poled and depoled P(VDF-TrFE)/OFET sensors can also be used for the measurement of static/quasi-static temperature, as demonstrated in Figs. 3 and 4. Fig. 3 confirms that higher temperature leads to an increased voltage on the gate of the transistor $|V_G|$ that consequently leads to higher drain current $|I_D|$ and higher $|V_{OUT}|$. While V_G remains constant for constant temperature, a gradual decrease in $|V_{OUT}|$ is observed as a result of the bias stress effect of the transistor [23,27]. Therefore, it is desirable to replace the DC input voltage with a pulsed V_{IN}. In addition, a low sampling rate can be used, thus minimizing the OFET bias stress effect. Application of a pulsed V_{IN} is demonstrated in Figs. 3 and 4 for the poled and depoled P(VDF-TrFE)/OFET sensor, respectively.

The output voltage $|V_{OUT}|$ of both the poled and depoled P(VDF-TrFE)/OFET sensors increases linearly with temperature (20–25 °C). Sensitivities of 3.8 and 17.2 mV/°C were achieved for depoled and poled P(VDF-TrFE) when OFETs with field-effect mobilities of 0.02 and 0.30 cm^2/Vs were used, respectively. This demonstrates that even the low-mobility transistors can be used if one would sacrifice the sensitivity. Assuming that the ferroelectricity does not affect $|V_{OUT}|$ during the measurement of static temperature, the transistor with higher μ and lower $|V_t|$ again leads to higher sensitivity of the sensor.

To obtain a detailed analysis of the response of P(VDF-TrFE)/OFET sensor to static or dynamic force or temperature, one would need to involve dynamic modelling of OFETs and ferroelectric capacitors. Here we would like to present a simple analytical model that describes the P(VDF-TrFE)/OFET sensor in steady-state condition. This model relies solely on capacitances because the d.c. leakage current of P(VDF-TrFE) capacitor is extremely small, amounting to a few pA at 1 V. A similar approach has been suggested previously [16,28], although in such cases the voltage on the gate of the transistor was set via a control capacitor, while in this case the transistor gate is floating. Assuming that the P(VDF-TrFE) capacitor behaves like any ordinary capacitor, the voltage on the gate of the transistor (see Fig. 1(c)) can be written

$$V_G = \frac{C_{PVDF}}{C_{TOT}} \cdot V_{IN} + \frac{C_{GD}}{C_{TOT}} \cdot V_D + \frac{C_{GS}}{C_{TOT}} \cdot V_{OUT} \quad (1)$$

where C_{PVDF} is the capacitance of P(VDF-TrFE), C_{GD} and C_{GS} are the gate/drain and gate/source overlap capacitances of the transistor, respectively, and $C_{TOT} = C_{PVDF} + C_{GD} + C_{GS}$. Based on Eq. (1), the changing C_{PVDF} should lead to a change in V_G; any change in V_G is manifested as a change in the drain current I_D of the transistor, and thus the output voltage V_{OUT} of the sensor. Eq. (1) holds true if the effect of the transistor channel can be neglected or the channel pinch-off point is located close to the source. Two alternative expressions for V_G were derived for transistor operating in the linear regime or at the onset of saturation. The comparison of all three expressions showed that V_G values differ less than 2%. Therefore, Eq. (1) is used in the following discussion because it simplifies the calculations.

To confirm that Eq. (1) fundamentally describes the behavior of the P(VDF-TrFE)/OFET sensor, the steady-state values of V_G and V_{OUT} were recorded for two P(VDF-TrFE)/OFET sensors and they are shown in Table 1. Transistors with different field-effect mobilities and two different sensors were chosen, leading to different values of V_G and V_{OUT}. The last column shows the values of V_G that were calculated using Eq. (1). The difference between the measured and calculated V_G is less than 5%.

Fig. 6(a) shows two measured p-channel transistor transfer characteristics in saturation. One corresponds to transistor with grounded source while for the other a 1 MΩ resistor was added between the source and ground. The addition of the resistor reduces the drain

Table 1
Validation of Eq. (1) for P(VDF-TrFE)/OFET sensor of Fig. 1(c). The Au-side of P(VDF-TrFE) was connected to the gate of the transistor and $V_{IN} = V_D = -2$ V. ($C_{GD} = C_{GS} = 776$ pF).

	μ (cm^2/Vs) OFET	V_G (V) measured	V_{OUT} (V) measured	V_G (V) calculated
P(VDF-TrFE)/OFET#1	0.56	−1.51	−0.68	−1.58
P(VDF-TrFE)/OFET#2	0.025	−1.38	−0.0051	−1.36

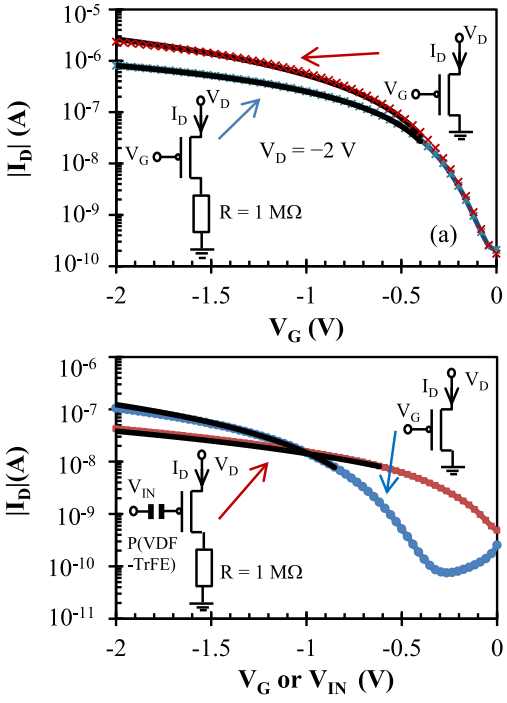

Fig. 6. Measured and calculated (solid black curves, Eqs. (2) and (4)) OFET drain current for R = 0 and 1 MΩ (a); measured and calculated (solid black curves, Eqs. (2) and (5)) drain current of OFET and P(VDF-TrFE)/OFET sensor measured at room temperature with zero force (b).

current and the respective drain currents in the saturation regimes can be written:

$$I_D = -\frac{W}{2L}C\mu(V_G - V_t)^2 \tag{2}$$

$$I_D = -\frac{W}{2L}C\mu(V_G - RI_D - V_t)^2 \tag{3}$$

where I_D is the transistor drain current, V_G the gate voltage, V_t the threshold voltage, C the gate dielectric capacitance per unit area, μ the field-effect mobility, W and L the transistor dimensions, and R the source resistor. Isolating I_D from Eq. (3) leads to

$$I_D = \frac{V_G - V_t}{R} - \frac{L}{WC\mu R^2} + \sqrt{-\frac{V_G - V_t}{R}\cdot\frac{2L}{WC\mu R^2} + \left(\frac{L}{WC\mu R^2}\right)^2} \tag{4}$$

Equations (2) and (4) were used to fit the measured I_D in Fig. 6(a) and the results are shown with solid black curves.

To derive the expression for P(VDF-TrFE)/OFET sensor of Fig. 1(c), one combines Eqs. (1) and (3). In such a case the drain current I_D is

$$I_D = \frac{-AC_{TOT}^2}{R^2(C_{TOT} - C_{GS})^2} - \frac{C_{TOT}V_t - C_{PVDF}V_{IN} - C_{GD}V_D}{R(C_{TOT} - C_{GS})} + \sqrt{\left[\frac{AC_{TOT}^2}{R^2(C_{TOT} - C_{GS})^2}\right]^2 + \frac{2AC_{TOT}^2}{R^2(C_{TOT} - C_{GS})^2}\cdot\frac{(C_{TOT}V_t - C_{PVDF}V_{IN} - C_{GD}V_D)}{R(C_{TOT} - C_{GS})}} \tag{5}$$

where $A = \frac{L}{WC\mu}$. Fig. 6(b) depicts the measured drain current of a transistor and P(VDF-TrFE)/OFET sensor based on this transistor. Again, the solid black curves represent the fits obtained from Eqs. (2) and (5). The agreement between the measured and calculated values presented in Table 1 and Fig. 6 represents the first step toward a future, more detailed model.

The circuit of Fig. 1(c) should also respond to dynamic force or temperature via the inherent piezo- or pyroelectric effect of the ferroelectric P(VDF-TrFE) layer, as illustrated in Fig. 5(a). In such a case Eq. (1) can be modified as follows [28].

$$V_G = \frac{C_{PVDF}}{C_{TOT}}\cdot V_{IN} + \frac{C_{GD}}{C_{TOT}}\cdot V_D + \frac{C_{GS}}{C_{TOT}}\cdot V_{OUT} + \frac{Q}{C_{TOT}} \tag{6}$$

where Q is the generated piezo/pyroelectric charge. In Fig. 5(a) the orientation of the poled P(VDF-TrFE) capacitor led to an increase (decrease) in $|V_{OUT}|$ with rising (falling) temperature. Changing the orientation of the capacitor led to an opposite effect, i.e. a decrease (increase) in $|V_{OUT}|$ with rising (falling) temperature. Depoled P(VDF-TrFE) in the paraelectric state cannot respond to changes in temperature via the pyroelectric effect ($\frac{Q}{C_{TOT}} = 0$) and any change in the sensor output voltage results from the change in P(VDF-TrFE) capacitance, as shown in Fig. 5(c) and discussed above.

The presented results suggest that the response from poled P(VDF-TrFE)/OFET sensor is a combination of P(VDF-TrFE) pyroelectric properties and a change in its capacitance, with the pyroelectric response being stronger. The response of depoled P(VDF-TrFE)/OFET sensor results from a change in P(VDF-TrFE) capacitance only. Consequently, a comparison of the output from P(VDF-TrFE)/OFET sensor in ferroelectric and paraelectric states to temperature stimulus may provide a route for separating the contributions from pyroelectricity and the change in capacitance. In a similar manner, one would expect that depoled P(VDF-TrFE)/OFET would not respond to dynamic force via piezoelectricity and any change in the output voltage with force would result from the change in capacitance. By comparing the output from P(VDF-TrFE)/OFET in ferroelectric and paraelectric states to a force stimulus, the contributions from the capacitance and piezoelectricity to the output could be separated. Thus, the choice of P(VDF-TrFE) layer (ferroelectric versus paraelectric) allows triggering of the desired response, thereby presenting a path for differentiation between the static and dynamic stimuli.

5. Conclusions

We showed that a multifunctional sensor can be produced by connecting a P(VDF-TrFE) capacitor to the gate of an organic field-effect transistor. Such sensor is able to respond to static/quasi-static or dynamic force or temperature. The dynamic response is achieved primarily through the piezoelectric (dynamic force) and pyroelectric (dynamic temperature) effects that are inherent within ferroelectric P(VDF-TrFE). Sensing of static force or temperature is linked to the capacitance of P(VDF-TrFE) that exhibits a change with force or temperature. This change in capacitance manifests itself as a change in the gate voltage of the transistor and, consequently, a change in the drain current and the output voltage from the sensor.

The output voltage of the P(VDF-TrFE)/OFET sensor exhibits a logarithmic response to static compressive force, leading to high sensitivity for small forces. This is consistent with the fact that the capacitance of the P(VDF-TrFE) layer exhibits a logarithmic increase with rising force. Such behavior is observed for both poled (ferroelectric) and depoled (paraelectric) P(VDF-TrFE)/OFET sensors. The poled and

depoled P(VDF-TrFE)/OFET sensor exhibited sensitivity of ~65 mV/N and ~20 mV/N for forces less than 0.1 N, respectively. The reduced sensitivity of the latter is ascribed to lower μ and higher $|V_t|$ of the transistor.

The output voltage of the P(VDF-TrFE)/OFET sensor exhibits a linear response to static/constant temperature regardless of whether P(VDF-TrFE) is in the ferroelectric or paraelectric state. Sensitivities ranging from 3.8 mV/°C to 17.2 mV/°C have been obtained in the measured temperature range from 20 to 25 °C. Again, correlation between better transistor performance and higher sensitivity is observed.

In addition, it has been confirmed that both poled and depoled P(VDF-TrFE)/OFET sensors respond to dynamic/changing temperature. However, the magnitude of the response, measured by the change in the output voltage, is dramatically different. While the majority of the response for the poled P(VDF-TrFE)/OFET sensor comes from the pyroelectric effect, the response of the depoled sensor is linked to the changes in capacitance of P(VDF-TrFE), and therefore, is much smaller. Nevertheless, the different 'mechanisms' of sensing the dynamic versus static temperature could be exploited for the separation of the two. A similar situation would occur for the dynamic versus static force.

Finally, this comprehensive study paves the way towards the development of multifunctional force and temperature sensors for e-skin or e-textiles based on a single ferroelectric polymer. The sensitivity of the sensor could be further enhanced by employing organic transistors with improved performance.

Acknowledgements

S.H. is a recipient of Doctoral Training Grant funded by the Engineering and Physical Sciences Research Council (EPSRC, EP/L505080/1). This project has received some funding from the European Union's Horizon 2020 research and innovation program under the Marie Skłodowska-Curie grant agreement No 734331.

References

[1] S. Wagner, S. Lacour, J. Jones, P. Hsu, J. Sturm, T. Li, Z. Suo, Phys. E Low-dimens. Syst. Nanostruct. 25 (2004) 326.
[2] C. Chang, F. Lee, Y. Lin, Y. Yang, 29th Int. Conf. on Microelectromechanical Systems, 2016, p. 169 Shanghai.
[3] J. Park, Y. Lee, S. Lim, Y. Lee, Y. Jung, H. Lim, H. Ko, BioNanoScience 4 (2014) 349.
[4] D. Thuau, M. Abbas, S. Chambon, P. Tardy, G. Wantz, P. Poulin, L. Hirsch, I. Dufour, C. Ayela, Org. Electron. 15 (2014) 3096.
[5] Y. Wang, J. Zheng, G. Ren, P. Zhang, C. Xu, Smart Mater. Struct. 20 (2011) 045009.
[6] L. Wang, L. Qin, L. Li, IEEE Int. Conf. On Information and Automation, 2010, p. 906.
[7] D. Thuau, M. Abbas, G. Wantz, P. Poulin, L. Hirsch, I. Dufour, C. Ayela, Sci. Rep. 6 (2016) 38672.
[8] N.T. Tien, S. Jeon, D.-I. Kim, T.Q. Trung, M. Jang, B.-U. Hwang, K.-E. Byun, J. Bae, E. Lee, J.B.-H. Tok, Z. Bao, N.-E. Lee, J.-J. Park, Adv. Mater. 26 (2014) 796.
[9] N. Marsi, B. Majlis, A. Hamzah, F. Mohd-Yasin, 2nd Int. Conf. On Sustainable Energy Engineering and Applications, 2014 Bandung, Indonesia.
[10] E.G. Bakhoum, M.H. Cheng, J. Microelectromech. Syst 19 (2010) 443.
[11] R. Dahiya, D. Cattin, A. Adami, C. Collini, L. Barboni, M. Valle, L. Lorenzelli, R. Oboe, G. Metta, F. Brunetti, IEEE Sens. J. 11 (2011) 3216.
[12] A. Kimoto, S. Shimada, IEEE Trans. Instrum. Meas. 62 (2013) 2870.
[13] A. Spanu, L. Pinna, F. Viola, L. Seminara, M. Valle, A. Bonfiglio, P. Cosseddu, Org. Electron. 36 (2016) 57.
[14] P. Cosseddu, F. Viola, S. Lai, L. Raffo, A. Bonfiglio, IEEE Electron Dev. Lett. 35 (2014) 1296.
[15] M. Zirkl, A. Sawatdee, U. Helbig, M. Krause, G. Scheipl, E. Kraker, P.A. Ersman, D. Nilsson, D. Platt, P. Bodö, S. Bauer, G. Domann, B. Stadlober, Adv. Mater. 23 (2011) 2069.
[16] I. Graz, M. Kaltenbrunner, C. Keplinger, R. Schwodiauer, S. Bauer, S.P. Lacour, S. Wagner, Appl. Phys. Lett. (2006) 89 073501.
[17] R. Dahiya, M. Valle, G. Metta, L. Lorenzelli, A. Adami, Appl. Phys. Lett. (2009) 95 034105.
[18] N.T. Tien, T.Q. Trung, Y.G. Seoul, D.I. Kim, N.-E. Lee, ACS Nano 5 (2011) 7069.
[19] T.Q. Trung, N.T. Tien, Y.G. Seol, D.I. Kim, N.-E. Lee, Org. Electron. 13 (2012) 533.
[20] S. Hannah, S. Khan, D. Uttamchandani, R. Dahiya, H. Gleskova, 11th Int. Conf. On PhD Research in Microelectronics and Electronics (PRIME), 2015 Glasgow.
[21] R. Dahiya, M. Valle, G. Metta, L. Lorenzelli, S. Pedrotti, 2008 IEEE Sensors, 2008, p. 490.
[22] H.S. Nalwa, Ferroelectric Polymers - Chemistry, Physics and Applications, Marcel Dekker Inc., New York, 1995.
[23] S. Hannah, J. Cardona, D. Lamprou, P. Sutta, P. Baran, A. Ruzaiqi, K. Johnston, H. Gleskova, ACS Appl. Mater. Interfaces 8 (2016) 25405.
[24] C.G. Nunez, W.T. Navaraj, E.O. Polat, R. Dahiya, Adv. Funct. Mater. 27 (2017) 1606287.
[25] R. Dahiya, M. Valle, Robotic Tactile Sensing: Technologies and System, Springer Science + Business Media, Dordrecht, 2013, pp. 1–245.
[26] Z.H. Liu, P. Maréchal, R. Jérôme, Polymer 39 (1998) 1779.
[27] S.J. Zilker, C. Detcheverry, E. Cantatore, D.M. De Leeuw, Appl. Phys. Lett. 79 (2001) 1124.
[28] A. Spanu, S. Lai, P. Cosseddu, M. Tedesco, S. Martinoia, A. Bonfiglio, Sci. Rep. 5 (2015) 8807.